Refractory Neuron Circuits

Rahul Sarpeshkar, Lloyd Watts, Carver Mead

California Institute of Technology
Pasadena, CA 91125

email: rahul@pcmp.caltech.edu

CNS Technical Report Number CNS-TR-92-08

Abstract

Neural networks typically use an abstraction of the behaviour of a biological neuron, in which the continuously varying mean firing rate of the neuron is presumed to carry information about the neuron's time-varying state of excitation. However, the detailed timing of action potentials is known to be important in many biological systems. To build electronic models of such systems, one must have well-characterized neuron circuits that capture the essential behaviour of real neurons in biological systems. In this paper, we describe two simple and compact circuits that fire narrow action potentials with controllable thresholds, pulse widths, and refractory periods. Both circuits are well suited as high-level abstractions of spiking neurons. We have used the first circuit to generate action potentials from a current input, and have used the second circuit to delay and propagate action potentials in an axon delay line. The circuit mechanisms are derived from the behaviour of sodium and potassium conductances in nerve membranes of biological neurons. The first circuit models behaviours at the axon hillock; the second circuit models behaviour at the node of Ranvier in biological neurons. The circuits have been implemented in a 2-micron double-poly CMOS process. Results are presented from working chips.

1 Introduction

Biological neurons typically communicate with each other via narrow fixed-amplitude pulses in membrane potential known as *action potentials*, nerve spikes, or spikes. In this discrete-amplitude continuous-time communication mechanism, noise immunity is achieved by a coarse amplitude quantization, while detailed timing information is preserved. The neurons have a practical upper limit on their firing frequency, which is controlled by their *refractory period*, a period following the firing of a pulse during which the threshold for the firing of a subsequent pulse is increased. The spikes propagate like waves along lengths of nerve fiber called *axons*, the output wires of neurons. The spikes originate at the start of the axon in the *axon hillock*, the part of the axon close to the *soma* or cell body of the neuron. The axons are typically insulated with *myelin* all along their length except at certain sites along their length called *nodes of Ranvier*. The action potentials propagate down the axon, being constantly boosted and prevented from dying out by regenerative circuits at the nodes of Ranvier.

Artificial neural networks typically use an abstraction of real neuron behaviour, in which the continuously varying mean firing rate of the neuron is presumed to carry the information about the neuron's time-varying state of excitation [1]. This useful simplification allows the neuron's state to be represented as a time-varying continuous-amplitude quantity. However, spike timing is known to be important in many biological systems. For example, in nearly all vertebrate auditory systems, spiral ganglion cells from the cochlea are known to phase lock to pure-tone stimuli for all but the highest perceptible frequencies [2]. The barn owl uses axonal delays to compute azimuthal spatial localization [3]. Studies in the cat [4] have shown that relative timing of spikes is preserved even at the highest cortical levels. Studies in the visual system of the blowfly [5] have shown that information in just three spikes is enough for the fly to make a decision to turn, if the visual input is sparse.

Interest in modeling pulsed neural systems in silicon has been growing. Early work on pulse coding and pulse computation in the neural-network context was done by Murray and Smith in 1987 [6]. In 1988, Ryckebusch, Mead, and Bower [7] described small oscillatory networks, consisting of simple spiking neurons, to model central pattern generators in invertebrates. The neuron circuit that they used allowed control of the firing frequency and pulse-width of the action potential; it is analyzed by Mead [8]. This neuron circuit has been used successfully in silicon models of auditory localization [9] and the jamming-avoidance response of the weakly electric fish *eigenmannia* [10]. A sophisticated silicon neuron model was introduced by Mahowald and Douglas in 1991 [11]; it modeled in great detail the behaviour of cortical neurons, including specific circuits for different ion conductances and adaptation mechanisms.

An important issue in silicon neuron modeling is the tradeoff between the degree to which biological behavior is realistically modeled and the number of parameters that must be specified for each neuron. Each parameter is usually specified by an externally applied bias voltage, which must be routed to the neuron on a wire of nonzero width. To prevent the layout area of a large network from becoming dominated by these bias wires, it is desirable to minimize the number of parameters required for each neuron. At the same time, the abstraction of neural behaviour

must not be so simple that essential biological characteristics are lost in the abstraction. In this paper, we describe two simple and compact neuron circuits that feature biologically realistic spiking behaviour. The circuits use eight and nine transistors, respectively, and have three bias-control knobs to set the threshold for firing, pulse-width, and refractory period of the action potential. We have used the first circuit to generate action potentials and have used the second circuit to delay and propagate them in an axon delay line.

The circuits are inspired by models of conductances in biological nerve membranes as modeled by Hodgkin and Huxley in 1952 [12] for a squid giant axon, and by Chiu et al. in 1979 [13] for a rabbit axon. We emphasize at the outset that the circuits are not intended to be detailed models of the biology, but rather are *efficient* silicon implementations of the ideas in these models. In Section 2, we describe the mechanisms behind the operation of the biological conductances. In Section 3, we describe and analyze the two neuron circuits. We present data from working chips for both of these circuits. In Section 4, we discuss applications of the two circuits. Finally, in Section 5, we conclude by summarizing the contributions of this work.

2 Biological Neurons

Hodgkin and Huxley [12] described the generation of action potentials in the surface membrane of a giant nerve fiber in the squid under the injection of a sufficiently large current. They showed that the dynamics behind the action potential could be explained completely by the presence of a quickly activating, transient sodium conductance that was responsible for the excitatory rise of the action potential and by a slowly activating, persistent potassium conductance that was responsible for the fall of the action potential. The extent to which these conductances were turned on (near their maximum values) was membrane-potential dependent. Further, the time constants governing the activation and inactivation of these conductances also were membrane-potential dependent. In this section, we give an intuitive and simplified explanation of their model as adapted from Kandel and Schwarz [14].

Figure 1 is a schematic of the conductances in the Hodgkin–Huxley model. The sodium conductance, may be viewed as being controlled by two gates in series, an m gate and an h gate. For the sodium conductance to turn on and to supply excitatory current, both the m and h gates must be open. The m gate opens rapidly at high membrane potentials and closes quickly at low membrane potentials. The h gate closes somewhat less quickly at high membrane potentials and opens slowly at low membrane potentials. If the sodium conductance is strongly turned on, the membrane potential is driven towards the sodium reversal potential, E_{Na}, the V_{DD} rail of neurobiology.

The potassium conductance may be viewed as being controlled by a single n gate. For the potassium conductance to turn on and to supply inhibitory current, the n gate must be open. The n gate opens with a delay at high membrane potentials and closes slowly at low membrane potentials. If the potassium conductance is strongly turned on, the membrane potential is driven towards the potassium reversal potential, E_K, the ground rail of neurobiology.

Table 1: Approximate time constants for gate opening and closing (in ms.).

Gate/Action	m	h	n
Opening	0.1	8	1
Closing	0.5	1	6

Besides the active (voltage-dependent) sodium and potassium conductances, there is also a passive (non–voltage-dependent) conductance present that ensures that the membrane potential remains at a low resting value, E_R, when the active conductances are turned off. This conductance is referred to as a leak conductance. Typically, the membrane resting potential, E_R, is close to the potassium reversal potential, E_K.

The time constants for the opening and closing of the m, h and n gates are taken from Hille [15] and tabulated in Table 1. Note that these numbers refer to the time constants at the extremes of the membrane potential, that is with the membrane potential at the low resting value near E_K, and with the membrane potential near the high sodium reversal potential E_{Na}; they *do not* represent the actual times taken to open or close the gates.

Before the start of an action potential, the membrane is at the resting potential, E_R and the m gate of sodium and the n gate of potassium are closed, whereas the h gate of sodium is open. If the membrane is driven sufficiently positive by an excitatory input, the m gate opens rapidly and sodium current rushes in to drive the membrane even more positive. The resulting positive-feedback action drives the membrane potential toward the high sodium reversal potential, E_{Na}. The sodium h gate now closes, because of the high membrane potential. The closure of the h gate shuts off the sodium conductance. Meanwhile, the more slowly activating n gate opens and, along with the passive leak, brings the membrane potential back to its low resting value, E_R. The low membrane potential closes the m gate quickly, but the n gate is slower in closing and closes only some time later. The sodium conductance cannot turn on until the h gate opens again. The h gate is slow to open, and does not open until well after the action potential is over and consequently causes a refractory period. Note that the refractoriness arises from two sources—the lack of excitability from the sodium channel since the h gate is slow to open, and the presence of inhibition from the potassium channel since the n gate is slow to close. The presence of potassium inhibition increases the refractoriness after the action potential, but the lack of sodium excitability is the primary determinant of the refractory period as the latter has a slower time course and persists even after the potassium inhibition has turned off.

Chiu et al. [13] showed that, at the nodes of Ranvier of a myelinated rabbit axon, action potentials were generated when a sodium conductance and a strong passive leak conductance with no potassium conductance were present. The transient sodium conductance was responsible for the excitatory rise of the action potential as before, and the strong leak conductance was responsible for quickly restoring the membrane potential to rest and keeping the action potential brief. Thus, the need for potassium conductances is obviated if strong leak conductances are

present.

The first of our neuron circuits in Section 3 is loosely like the Hodgkin–Huxley sodium-potassium conductance pair. We refer to it as the "sodium-potassium neuron". We primarily designed it as an efficient engineering solution to the problem of creating a refractory period after the firing of a pulse. The biological equivalent of this neuron would be as follows. A persistent sodium conductance (one that has only an m gate and no h gate) causes the rising phase of the action potential. The sodium conductance activates, after a delay, a potassium conductance that is coupled to it. This potassium conductance restores the membrane potential to rest and causes the falling phase of the action potential. The potassium conductance inactivates slowly, so the persistence of potassium inhibition causes a refractory period after the firing of the action potential. Sodium and potassium conductances are usually present at axon-hillock locations in biological neurons, and one can generate action potentials by injecting current at these locations. The circuit, therefore, bears some similarity to biological axon-hillock circuits.

The second of our neuron circuits described in Section 3 models a transient sodium conductance and a leak to generate action potentials. We refer to it as the "sodium-leak neuron". The transient sodium conductance in the circuit has close similarities to the Hodgkin–Huxley sodium-conductance model, and the m and h gates are modeled directly by transistors in the circuit. The overall circuit is quite like the biological rabbit node of Ranvier circuit of Chiu et al. [13], which also has only leak and transient sodium conductances, and no potassium conductance.

3 Silicon Neurons

In this section, we describe, analyze and present data for the two neuron circuits. In Section 3.1 we review briefly the equations in the subthreshold region of operation of an MOS transistor, which is where we primarily operate our circuits. In Section 3.2, we discuss the sodium-potassium neuron circuit. In Section 3.3 we discuss the sodium-leak neuron circuit. Both the sodium-potassium neuron circuit and the sodium-leak neuron circuit have three bias voltages to control the threshold, pulse width, and refractory period of the action potential.

The sodium-potassium neuron circuit takes as its input a current, and generates as its output a train of pulses from ground to V_{DD}. The pulses are fired only if the current charges the input (and output) node higher than the threshold voltage. The firing frequency increases with input current until the upper frequency limit set by the refractory period is reached; for larger inputs the firing frequency saturates.

The sodium-leak neuron circuit takes as its input a positive step change in voltage, and generates as its output a pulse from ground to V_{DD}. The pulse is generated only if the height of the input step is greater than a threshold voltage. The voltage input is coupled capacitively to the input (and output) node of the neuron. The circuit is thus like a thresholding positive-edge triggered oneshot; it fires a pulse on every positive edge of a square-wave input and remains dormant on every negative edge. However, because of the circuit's refractory properties, as the frequency of the square wave is increased, the firing shifts from ocurring on every edge to on

every other edge, to on every third edge, and so on.

3.1 Review of Transistor Operation in Subthreshold

In the subthreshold region of operation, the current, I_{ds}, flowing through an nMOS transistor from drain to source is given by

$$I_{ds} = I_0 e^{\frac{\kappa V_g}{U_T}} \left(e^{-\frac{V_s}{U_T}} - e^{-\frac{V_d}{U_T}} \right) \tag{1}$$

where V_g is the gate voltage, V_d is the drain voltage, V_s is the source voltage, $U_T = \frac{kT}{q}$ is the thermal voltage, and I_0, and κ are constants [8]. For pMOS transistors, Eq. 1 is valid if all voltages are measured downward from V_{DD} ($V \rightarrow V_{DD} - V$). The parameter κ is usually lower for transistors in the well than for transistors in the substrate, and typically lies between 0.5 and 0.9. The parameter I_0 is different for every transistor, and scales with the width-to-length ratio of the transistor. If $V_d - V_s \gg 5U_T$, Eq. 1 simplifies to

$$I_{ds} = I_0 e^{\frac{\kappa V_g - V_s}{U_T}}. \tag{2}$$

The subthreshold equations are valid in the region where

$$\kappa V_g - V_s < V_T. \tag{3}$$

The parameter V_T is called the transistor threshold voltage. For the process in which our chips are fabricated, the threshold voltage V_T was approximately 0.9 V for both $n-$ and $p-$channel transistors.

3.2 The Sodium-Potassium Neuron

In Sections 3.2.1 and 3.2.2, we describe and analyze the sodium-potassium neuron circuit. In Section 3.2.3 we present experimental data for this neuron.

3.2.1 Circuit Description and Operation

The sodium-potassium neuron circuit is shown in Figure 2. The capacitance C_m represents the neuron membrane capacitance. The voltage V_m represents the membrane potential. The input current to the circuit is I_{in}. The sodium conductance behaviour is modeled by transistors ND, NM_1, NM_2, PM_1 and PM_2. A higher membrane potential increases I_{M1}, which is mirrored to form the excitatory sodium current I_{Na}. The mirror transistors are sized such that $I_{Na} = 3I_{M1}$ and $I_{MC} = \frac{I_{M1}}{3}$. The voltage V_{Na}^{th} sets the threshold of activation of the sodium conductance and thereby controls the threshold for firing of the neuron. The current I_{Na}^{max}, set by the voltage V_{Na}^{max} controls the maximum sodium current and determines the pulse width of the action potential.

The potassium-conductance behaviour is modeled by transistors NK and NR. The voltage V_n on capacitor C_N represents the state of activation of the potassium conductance. The larger V_n is, the stronger is the inhibitory potassium current, I_K, and the more refractory is the neuron. The transistor PM_C couples the sodium and potassium conductances, such that C_N is charged high whenever there is sodium current present. The current I_R, set by the voltage V_R, controls the refractory period of the neuron.

Initially, we assume that the membrane capacitance is discharged ($V_m = 0$) and that the neuron is not in a refractory state ($V_n = 0$). Since $V_m < V_{Na}^{th}$, nearly all the current I_{Na}^{max} flows in the right side of the differential pair. The input current I_{in} charges C_m until $V_m > V_{Na}^{th}$. At this point, the current I_{Na}^{max} flows predominantly in the left side of the differential pair, so $I_{M1} = I_{Na}^{max}$, and the current mirror causes the additional current $I_{Na} = 3I_{Na}^{max}$ to charge C_m. After the threshold voltage V_{Na}^{th} is reached, the resulting positive feedback charges V_m quickly toward V_{DD}.

The current I_{MC} is activated at the same time as I_{Na}; this current causes V_n to rise by charging C_N. When V_n is large enough to cause a current $I_K > I_{Na} + I_{in}$ to flow, I_K pulls V_m down toward ground, completing the action potential. The mirror transistor ratio $I_{Na}/I_{MC} = 9$ ensures that a full-blown action potential occurs. Once $V_m < V_{Na}^{th}$, both I_{Na} and I_{MC} are deactivated. As long as V_n is large enough to keep $I_K > I_{in}$, V_m remains discharged and the neuron is in its refractory period. V_n is leaked away to ground by the current source I_R, which controls the duration of the refractory period. Once V_n becomes small enough that $I_K < I_{in}$, the refractory period is over and I_{in} is capable of initiating another action potential.

3.2.2 Circuit Analysis

The controlling parameters for the circuit are the voltage V_{Na}^{th}, which controls the threshold voltage, the current I_{Na}^{max} which controls the pulse-width of the action potential, and the current I_R, which controls the duration of the refractory period. We expect that, under normal operation, the current $I_{Na}^{max} \gg I_{in}$, i.e. that the positive-feedback current will overwhelm the input current when an action potential is initiated.

We define the threshold for firing an action potential V_{TH} as the value of V_m such that the positive feedback current I_{Na} is equal to the input current I_{in}. It can easily be shown that

$$V_{TH} = V_{Na}^{th} - \frac{U_T}{\kappa} \ln \left(\frac{3I_{Na}^{max}}{I_{in}} - 1 \right), \tag{4}$$

where we assume that all transistors are operating below threshold. In general, $V_{TH} < V_{Na}^{th}$, because the positive-feedback current begins to make its contribution before V_m actually reaches V_{Na}^{th}.

The critical value for V_n is that value for which the pull-down current $I_K = I_{in} + 3I_{Na}^{max}$; when V_n reaches this critical voltage, V_n^{hi}, I_K will discharge C_m and cause the end of the action potential.

$$V_n^{hi} = \frac{U_T}{\kappa} \ln \left(\frac{3I_{Na}^{max} + I_{in}}{I_0} \right). \tag{5}$$

The pulse width, t_p, or the duration of the action potential, is the time required to charge up the capacitance C_N from ground to the critical value V_n^{hi}; it is given by

$$t_p = \frac{C_N V_n^{hi}}{\frac{I_{Na}^{max}}{3} - I_R}. \tag{6}$$

The circuit is usually operated in the region where $I_{Na}^{max} \gg I_R$, so the pulse-width is determined primarily by I_{Na}^{max}.

The refractory period is the time required for I_R to discharge C_N to a value V_n^{lo} such that the current I_K is equal to I_{in}. It is easy to show that V_n^{lo} is given by

$$V_n^{lo} = \frac{U_T}{\kappa} \ln\left(\frac{I_{in}}{I_0}\right). \tag{7}$$

The refractory period is

$$t_R = \frac{C_N\left(V_n^{hi} - V_n^{lo}\right)}{I_R} = \frac{C_N}{I_R}\frac{U_T}{\kappa} \ln\left(\frac{3I_{Na}^{max} + I_{in}}{I_{in}}\right), \tag{8}$$

where V_n^{hi} and V_n^{lo} are given by Eqs. 5, and 7, respectively.

3.2.3 Chip Data

Figure 3 shows the trajectories of the two voltages V_m and V_n. At the beginning of the trace, V_m increases linearly due to the constant current I_{in}, until V_m approaches V_{Na}^{th}, the threshold voltage; at this point, V_m is quickly charged up toward V_{DD}, and V_n begins to rise. A short time later, V_n is large enough to cause V_m to be pulled hard to ground, completing the action potential. V_n is then discharged slowly to ground by I_R, during which time the cell is in its refractory period and V_m is held low by the transistor NK.

Figure 4a shows the spike rate versus the input voltage V_{in} for several values of the refractory voltage V_R. Leakage currents place a lower limit on the spike rate of the neuron of about 0.03 Hz. As expected, the refractory period places an upper limit on the spike rate of the neuron.

Figure 4b shows the refractory period versus the control input V_R. As expected, the refractory period is an exponential function of V_R in the subthreshold region, with a slope of $\kappa q/(kT) = 27.16V^{-1}$, corresponding to $\kappa = 0.706$.

3.3 The Sodium-Leak Neuron

In Sections 3.3.1 and 3.3.2, we describe and analyze the circuit. In Section 3.4 we present experimental data for the circuit.

3.3.1 Circuit Description and Operation

Figure 5 shows the sodium-leak neuron circuit. The circuit has strong similarities to the Hodgkin–Huxley model of sodium conductance. The membrane potential, referred to ground, is denoted by V_m. The m gate is represented by transistor NM. The h gate is represented by transistor NH. The membrane potential V_m controls the state of the m gate such that, the larger V_m is, the more strongly turned on the m gate is. The membrane potential V_m controls the h gate through transistors NC and PC such that, the larger V_m is, the less strongly turned on the h gate is. The voltage on capacitor C_H represents the state of the h gate; it is denoted by V_h. The input to the circuit is V_{in}; it is capacitively coupled to the membrane potential via C_c. The voltages V_L, V_D, and V_R set the maximum currents flowing through transistors NL, ND and PR to be I_L, I_D, and I_R, respectively. The current I_L represents the passive leak current and determines a voltage threshold and rate threshold for firing an action potential, i.e. both the input voltage change, ΔV_{in}, and the input voltage's rate of change, $\frac{dV_{in}}{dt}$, must be sufficiently high for an action potential to be fired. Both these thresholds are increased if I_L is increased. The current I_D, along with capacitor C_H, determines the rate of closing of the h gate and thus sets the pulse width. The current I_R, along with capacitor C_H, determines the rate of opening of the h gate and thus sets the refractory period. The transistors PM_1 and PM_2 form a current mirror and represent the positive feedback action of the the sodium conductance. Note that, for excitatory current to flow out of PM_2 and to raise the potential of V_m, both the m gate and h gate must be turned on as transistors NM and NH are in series.

Experimental data in Figure 6 shows the dynamic behaviour of nodes V_{in}, V_m, and V_h while the circuit was generating a series of action potentials. When the circuit is at rest, the membrane potential V_m is at ground, V_{in} is unchanging, and V_h is at V_{DD}. Thus, as in the Hodgkin–Huxley sodium-conductance model, the m gate NM is closed and the h gate NH is open. If there is a positive step input of magnitude ΔV_{in} at the input, a capacitive surge of current will charge the membrane potential to ΔV_{in}. If ΔV_{in} is large enough, the current through the series combination of NM and NH will be larger than I_L and will be mirrored back through PM_1 and PM_2 to charge the membrane potential node. The rise in membrane potential will increase the current still further, since NM is turned on even more strongly. The resulting positive-feedback action will cause the membrane potential to be driven almost all the way to V_{DD}[1]. If, on the other hand, ΔV_{in} is not large enough, the current that is mirrored back through PM_1 and PM_2 will be smaller than I_L and the membrane potential will fall, causing transistor NM to be turned on more weakly. The positive feedback will now turn off NM completely and I_L will discharge the membrane potential back to ground. Thus, there is a threshold for firing at the input—a minimum ΔV_{in} is needed to excite the circuit to V_{DD}. This threshold is controlled by I_L or equivalently by V_L. A larger I_L implies a larger threshold. In addition to the voltage threshold discussed above, the input voltage's rate of change, $\frac{dV_{in}}{dt}$, must be sufficiently high so that voltage increases in V_{in} cause voltage increases in V_m through capacitor C_C, in spite of the inhibiting

[1]The voltage V_m, is driven to a value that is a few mV lower than V_{DD}, say, $V_{DD} - \epsilon$. The value ϵ is such that the current flowing through transistor PM_2, with a strongly turned on gate voltage, V_{mir}, and a small drain-to-source voltage, ϵ, is equal to I_L.

influence of I_L. The smaller the capacitor C_C and the larger the current I_L, the higher is the threshold on the rate of change of input voltage.

When V_m is at V_{DD}, transistor NC is turned on strongly and transistor PC is turned off. Thus, the current, I_D, discharges the capacitor C_H, and drives V_h away from V_{DD} and toward ground. Eventually, V_h will be low enough that the current through NM and NH will be less than I_L. The membrane potential will then begin to fall, and will be discharged back to ground by I_L. Thus, in response to a step of sufficient height, an action potential pulse will be generated. The pulse width is controlled primarily by the current I_D, or equivalently, by the voltage V_D, with a larger I_D implying a shorter pulse width. The pulse width is also weakly dependent on I_L, since a larger I_L will cause V_m to start falling sooner and at a higher value of V_h, so the pulse width will be shorter.

When V_m is near ground, transistor NC is turned off and transistor PC is turned on strongly. Now node V_h is charged back up to V_{DD} by the current I_R. The threshold for firing is high right after the firing of the action potential, since V_h is close to ground and NH is shut off. As V_h approaches V_{DD}, the threshold for firing decreases progressively. Thus, the action potential has a refractory period. The refractory period is controlled by I_R, or equivalently, by the voltage V_R, with a high I_R implying a short refractory period.

The circuit should be operated in the range where $\frac{I_L}{C_C} \gg \frac{I_D}{C_H} > \frac{I_R}{C_H}$. The inequality $\frac{I_L}{C_C} \gg \frac{I_D}{C_H}$ ensures that the falling edge of the action potential is brief and sharp, as compared with the rest of the pulse. The inequality $\frac{I_D}{C_H} > \frac{I_R}{C_H}$ makes the refractory period longer than the pulse width as it is in a biological action potential.

3.3.2 Circuit Analysis

In this section, we derive expressions for the dependence of the voltage threshold V_{TH} on V_L, the pulse width t_p on V_D, and the refractory period t_R on V_R. We always operate the circuit with voltages V_D and V_R at subthreshold voltages. It is important in this circuit, as in biology that the leak current be high so that the action potential is brief. For this reason, the leak voltage V_L is sometimes an above-threshold voltage. Our analysis is quantitative for the case where V_L is a subthreshold voltage and is qualitative for the case where V_L is an above-threshold voltage. We assume in the analysis below, that the step changes in the input are sufficiently steep so that

$$C_C \frac{dV_{in}}{dt} \gg I_L. \tag{9}$$

In effect, we are only modeling voltage threshold effects and neglecting rate threshold effects.

The threshold voltage, V_{TH}, is determined by that voltage, V_m, at which the current flowing through transistors NH, NM, PM_1, and PM_2 is I_L, given that V_h is at V_{DD} (if V_h is below V_{DD}, the circuit is within its refractory period and the threshold is higher than the value we are computing). If V_h is at V_{DD}, the source of transistor NM will be approximately at ground, since transistor NH behaves like a switch. The approximation that the source voltage of transistor

NM is at ground is an excellent approximation if V_L is a subthreshold voltage. If PM_1 and PM_2 are matched and NH and NL are matched, therefore, $V_m = V_L$ at threshold.

Due to the presence of parasitic capacitance present at the membrane potential node, the change in membrane potential, ΔV_m, due to a step voltage change of ΔV_{in} at the input node is given by

$$\Delta V_m = \left(\frac{C_c}{C_c + C_{par}}\right) \Delta V_{in}, \tag{10}$$

where C_{par} is the parasitic capacitance at the membrane potential node. Thus, the threshold measured at the input, V_{TH}, is given by

$$\boxed{V_{TH} = \left(\frac{C_{par}+C_c}{C_c}\right) V_L.} \tag{11}$$

If V_L is an above-threshold voltage, we can no longer make the approximation that transistor NH is a switch, and NH behaves like a nonlinear source-degeneration resistor that reduces the transconductance of transistor NM. For the current flowing through NM, NH, PM_1 and PM_2 to be I_L, therefore, the voltage V_m has to higher than it was in the subthreshold case. Thus, above threshold the V_{TH} vs. V_L curve is expected to be steeper than that predicted by Eq. 11 for the subthreshold region.

The pulse width t_p, is determined by the time taken to discharge V_h from V_{DD} to the value at which the current through NM, NH, PM_1, and PM_2 falls to I_L. Just before the pulse ends, $V_m = V_{DD}$. Thus, we may treat transistor NM as a switch, and approximate the current just before the pulse ends to be determined by the voltage V_h. If all transistors are matched, the point at which the current through transistors NM, NH, PM_1, and PM_2 falls to I_L, therefore occurs when $V_h = V_L$. This is an excellent approximation if V_L is a subthreshold voltage. Further, we know that V_h is discharged at the rate given by $\frac{I_D}{C_H}$. Thus, the pulse width is computed to be

$$\boxed{t_p = \frac{C_H(V_{DD}-V_L)}{I_D}.} \tag{12}$$

The current I_D is given by the subthreshold Eq. 2 for transistor ND. As in the case for determining V_{TH}, if V_L is above threshold, the approximation of transistor NH being a switch is no longer valid and the pulse width predicted from Eq. (12) is an overestimate, since V_h is greater than V_L at the point where V_m begins to fall.

The refractory period, t_R, is determined by the time taken to recharge V_h from its low value, V_h^{lo}, at the end of the pulse to a value, V_h^{hi}, that is sufficiently high that the current flowing through the chain of transistors NM, NH, PM_1 and PM_2 is I_L; that is,

$$\boxed{t_R = \frac{C_H\left(V_h^{hi}-V_h^{lo}\right)}{I_R}.} \tag{13}$$

In subthreshold, the current I_R is given by

$$I_R = I_0^{PR} e^{\frac{\kappa_p(V_{DD}-V_R)}{U_T}}, \tag{14}$$

where κ_p and I_0^{PR} are the κ and I_0 parameters for transistor PR. From the analysis to determine t_p, we know that $V_h^{lo} = V_L$ is an excellent approximation if V_L is a subthreshold voltage; it is an underestimate if V_L is an above-threshold voltage. The voltage V_h^{hi} is a function of how close ΔV_{in} is to the threshold V_{TH}. We now compute V_h^{hi} as a function of ΔV_{in} for V_L being a subthreshold voltage. We assume, for simplicity, that $C_{par} = 0$, $V_{OS} = 0$, and all transistors are matched. The current flowing through NM and NH may be shown to be

$$I_{mh} = \frac{I_0 e^{\frac{\kappa V_m}{U_T}} e^{\frac{\kappa V_h}{U_T}}}{e^{\frac{\kappa V_m}{U_T}} + e^{\frac{\kappa V_h}{U_T}}}, \tag{15}$$

where V_m and V_h are both sub-threshold voltages, Eq. 1 is valid for transistors NM and NH, and $V_{mir} \gg \frac{5kT}{q}$. The voltage V_h^{hi} is then the solution to the equation

$$I_{mh} = I_0 e^{\frac{\kappa V_L}{U_T}}, \tag{16}$$

with I_{mh} as defined in Eq. 15, $V_m = \Delta V_{in}$ and V_h being the unknown variable for which we must solve. Some algebraic manipulation yields,

$$V_h^{hi} = \Delta V_{in} - \frac{U_T}{\kappa} \ln\left(e^{\frac{\kappa(\Delta V_{in} - V_L)}{U_T}} - 1\right), \tag{17}$$

with $\Delta V_{in} > V_L$, so an action potential exists. The limiting cases of Eq. 17 yield

$$\lim_{\Delta V_{in} \to \infty} V_h^{hi} = V_L, \tag{18}$$

$$\lim_{\Delta V_{in} \to V_L} V_h^{hi} = \infty. \tag{19}$$

Note that the R.H.S. of Eq. (17) is a very steep function of ΔV_{in}. Within approximately $\frac{5kT}{q\kappa}$, which is about 0.2 V, it changes from ∞ to V_L. The two limiting cases are consistent with physical intuition about the circuit: If ΔV_{in} is very large, the point at which the current through transistors NM, NH, PM_1 and PM_2 is I_L occurs when $V_h \approx V_L$, since NH limits the current and NM is a switch. If ΔV_{in} is very near V_L, the point at which the current through transistors NM, NH, PM_1, and PM_2 is I_L occurs when V_h is very large, since NM limits the current and NH must be as perfect a switch as it can be. In practice, since we can never attain ∞, but rather can attain only V_{DD}, the lowest obtainable threshold has to be slightly greater than V_L; similarly, the lowest V_h^{hi} will have to be slightly greater than V_L. If V_L is an above-threshold voltage, Eq. 17 is not valid. The functional relation between V_h^{hi} and ΔV_{in}, however, has a similar form and Eqs. 18 and 19 are still true. The voltage V_h^{hi} is a monotonic decreasing function of ΔV_{in} that decreases from V_{DD} at $\Delta V_{in} \approx V_L$ to V_L at $\Delta V_{in} \approx V_{DD}$.

3.4 Chip Data

Data were taken from a chip containing the circuit of Figure 5. The data are shown in Figures 6–9. Circuit waveform data are shown in Figure 6 and were discussed in Section 3.3.1. The V_{TH}

versus V_L curve of Figure 7 was fit by the expression $1.6\,(V_L - 0.05)$ for the subthreshold range of voltages $0.5 < V_L < 0.85$ V. The data are consistent with Eq. 11, except for the presence of a small offset of 50 mV. The offset is partly due to transistor mismatch, partly because the function generator used to collect data had a slight overshoot in its square wave output and partly because V_m does not rest exactly at ground. We obtained independent measurements of the parasitic capacitance attenuation from V_{in} to V_m by taking the ratio of the peak-to-peak amplitudes of a sine wave at V_{in} and V_m respectively, with the circuit turned off (V_L at ground, V_D at V_{DD}, V_R at V_{DD}); they yielded a value of 1.58. The value of 1.58 compares very favorably with the value of 1.6 from data. Above threshold, the V_{TH} versus V_L curve deviates from the subthreshold fit curve and becomes increasingly steep as expected from the discussion that follows Eq. 11 in Section 3.3.2.

Equation 12 predicts that the t_p vs. V_D curve should decrease exponentially in the subthreshold regime; Figure 8 shows that this prediction is correct. The data points were fit to an exponential in the range $0.450 < V_D < 0.800$ with a κ of 0.68, which compares favorably with the $\kappa = 0.66$ value determined by an independent measurement on a test nMOS transistor on the same chip.

We obtained refractory period data by measuring the critical frequency, f_R, at which the circuit transitioned from firing on every rising edge of the input V_{in} (a square-wave input with frequency f_{in}) to firing on every other rising edge of the input, as a function of V_R. This frequency-halving behaviour is shown in Figure 9a. The experiment was performed with the magnitude of the positive step change in the input ΔV_{in} approximately equal to the threshold for firing, V_{TH}. This procedure yields the maximum possible refractory period as discussed in Section 3.3.2. The refractory period, t_R was then computed to be

$$t_R = \frac{1}{f_R} - t_p. \tag{20}$$

While taking these measurements, we always ensured that the input period, $\frac{1}{f_R}$, was greater than the pulse width, t_p; that is, as f_R increased with decreasing V_R, we simultaneously decreased t_p by increasing V_D. Figure 9b shows a plot of the data obtained for t_R versus V_R. As expected from Eq. 13, the data are exponential in the subthreshold regime. The data points in the range $4.25 < V_R < 4.65$ fit an exponential, with the κ parameter being 0.62. The κ determined by an independent measurement on a test pMOS transistor on the same chip was 0.56. This discrepancy was caused by the reduction of the threshold for firing with increasing frequency: As the frequency of the input is increased, the voltage at the gate of the mirror transistor PM_1, V_{mir}, has less time between successive inputs to charge back up to V_{DD}. Consequently, at higher frequencies, V_{mir} is at a lower voltage between action potentials and the current subtracted from transistor NL by transistor PM_2 is higher so the threshold is systematically lower. The lower threshold greatly reduces V_h^{hi} and, consequently, t_R, so the decrease of t_R with increasing frequency or decreasing V_R is made steeper. The κ parameter obtained from the data on t_R versus V_R is thus higher than one would expect from single-transistor measurements.

4 Circuit Applications

We have used the sodium-potassium neuron circuit in a number of applications that involve the processing of information from electronic cochleas [16] [17]. Phase and amplitude information from signals in the cochlea are processed by small neuronal-network circuits that model inner hair cells and spiral ganglion cells in real cochleas, and are encoded as phase-locked neuronal discharges, just as in biological auditory nerve fibers. The sodium-potassium neuron has been used in an auditory center-surround circuit to provide frequency sharpening, and in small networks that model the central pattern generator circuits involved in motor control in invertebrates [18].

Whereas the sodium-potassium neuron is naturally suited for generating spike trains and building networks, the sodium-leak neuron is naturally suited for propagating and delaying action potentials, and for doing delay computations. By inverting the output (the V_m node) of the sodium-leak neuron we obtain an active low positive-edge triggered oneshot. A cascade of such one-shots builds an axon delay line where the pulses are delayed at each succeeding stage by one pulse width. Data from such an axon delay line are shown in Figure 10. We have used the onset-detecting and delay-generating properties of the neuron to build a working chip that computes velocity estimates of locally moving edges in a 1D visual image [19]. The neuron has also been used in a working chip that recognizes sequences of two tones in an auditory input.

5 Conclusions

The two biologically inspired spiking neuron circuits that we have described and analyzed in this paper are robust, compact (eight to nine transistors), easily controllable, and operate over wide ranges in firing frequency, pulse width, refractory period and threshold. The firing frequency can be varied from a few tenths of 1 Hz. to 100 kHz. In the subthreshold region of operation, the pulse widths and/or refractory periods of the action potentials can be varied from a few tens of μsecs. to hundreds of msecs. The threshold for firing can be varied from approximately 0.7 V to V_{DD}. The power consumption of these circuits is low, since the circuits operate primarily in the subthreshold regime. The circuits are thus eminently suited for use as fundamental modules in pulsed-mode neural-network circuitry or as building blocks in the silicon modeling of neurobiological systems. We have used these circuits to build working electronic auditory nerve fibers, central pattern generators, axon delay lines, and visual motion detectors.

6 Acknowledgments

We gratefully acknowledge helpful discussions with Misha Mahowald and Rodney Douglas. This work was sponsored by the Office of Naval Research and the California State Competitive Technology Office. Chip fabrication was provided by the Defense Advanced Research Projects Agency and through the MOSIS Service.

References

[1] J. Hertz, A. Krogh and R. Palmer, *Introduction to the Theory of Neural Computation*, Addison-Wesley, 1991.

[2] N. Y-S. Kiang, T. Watanabe, E. C. Thomas, L. F. Clark, "Discharge Patterns of Single Fibers in the Cat's Auditory Nerve", MIT Res. Monograph No. 35, (MIT, Cambridge, MA).

[3] M. Konishi, T.T. Takahashi, H. Wagner, W.E. Sullivan, C.E. Carr, "Neurophysiological and Anatomical Substrates of Sound Localization in the Owl", In *Auditory Function*, G.M. Edelman, W.E. Gall, and W.M. Cowan, eds., pp. 721–745, Wiley, New York.

[4] D. P. Phillips and S. E. Hall, "Response Timing Constraints on the Cortical Representation of Sound Time Structure", Journal of the Acoustical Society of America, **88** (3), pp. 1403–1411, 1990.

[5] R.R. de Ruyter van Steveninck and W. Bialek, "Real-time Performance of a movement-sensitive neuron in the blowfly visual system: Coding and information transfer in short spike sequences", *Proceedings of the Royal Society of London, Series B*, **234**, 379-414.

[6] A.F. Murray and A.V.W. Smith,"A Novel Computational and Signaling Method for VLSI Neural Networks", . *Proc. European Solid State Circuits Conf.*, 1987, pp. 19–22.

[7] S. Ryckebusch, C. Mead, and J. Bower, "Modeling Small Oscillating Biological Networks in Analog VLSI", *Proc. Neural Information Process. Syst. Conf.*, Dec. 1988, pp. 384–393.

[8] C.A. Mead,*Analog VLSI and Neural Systems*, pp. 27-41, Addison-Wesley, Reading, MA, 1989.

[9] J. P. Lazzaro and C. Mead, "Silicon Models of Auditory Localization," Neural Computation 1, pp. 47–57, 1989.

[10] J.E. LeMoncheck, "An Analog VLSI Model of the Jamming Avoidance Response in Electric Fish", I.E.E.E Journal of Solid State Circuits **27**, No. 6, June 1992.

[11] M. Mahowald and R. Douglas,"A Silicon Neuron", NATURE, **354**, pp. 515–518, December 1991.

[12] A.L. Hodgkin. and A.F. Huxley, "A Quantitative Description of Membrane Current and Its Application to Conduction and Excitation in Nerve", Journal of Physiology, **117**, pp. 500–544, 1952.

[13] S.Y. Chiu, J.M. Ritchie, R.B. Bogart and D. Stagg (1979), "A Quantitative Description of Membrane Currents in Rabbit Myelinated Nerve", Journal of Physiology, **292**, pp. 149–166, 1979.

[14] E.R. Kandel and J.H. Schwartz, *Principles of Neural Science*, Second Ed., pp. 81–84, Elsevier Science, New York, 1985.

[15] B. Hille, *Ionic Channels of Excitable Membranes*, Fig. 17, pp. 47 and pp. 66–68, Sinauer Associates, Sunderland, MA, 1984.

[16] R.F. Lyon and C.A. Mead, "An Analog Electronic Cochlea", I.E.E.E. Transactions on Acoustics, Speech and Signal Processing, **36** (7), pp. 1119–1134, July 1988.

[17] L. Watts, D.A. Kerns, R.F. Lyon and C.A. Mead, "Improved Implementation of the Silicon Cochlea", I.E.E.E. Journal of Solid State Circuits, **27** (5), pp. 692–700, May 1992.

[18] L. Watts, "Designing Networks of Spiking Silicon Neurons and Synapses", to appear in CNS*92, Proceedings of Computation and Neural Systems Meeting, J. Bower, ed., July 1992.

[19] R. Sarpeshkar, W. Bair and C.Koch, "A Silicon Chip for Local Velocity Estimation based on Motion Detection in the Fly", submitted for publication to the Neural Information Processing Systems Conference, 1992.

Figure Captions

Figure 1—The Hodgkin–Huxley Conductance Model: The sodium conductance has m and h gates whose extent of opening is controlled by the membrane potential, V_m. The more open the m and h gates are, the larger the sodium conductance is. Similarly, the more open the n gate is, the larger the potassium conductance is. The leak conductance is non–voltage-dependent. The sodium, potassium and leak conductances are connected to voltage sources of value E_{Na}, E_K and E_R respectively.

Figure 2—The Sodium-Potassium Neuron Circuit: The voltage, V_m, on capacitor C_m is the membrane potential, and the voltage V_n on capacitor C_N is the voltage that determines the state of refractoriness of the neuron. The bias voltages V_{Na}^{th}, V_{Na}^{max} and V_R set the threshold for firing, pulse width, and refractory period of the action potential, respectively. The input current, I_{in}, determines the frequency of firing of the neuron, as long as it is not limited by the neuron's refractory period.

Figure 3—Circuit Waveforms for the Sodium-Potassium Neuron Circuit: The voltage V_m increases linearly with time, as the capacitor C_m is charged up by the input current from ground to the threshold for firing. When the threshold for firing is reached, the positive feedback in the circuit is activated and V_m quickly rises toward V_{DD}. At the threshold for firing, the voltage, V_n, also rises quickly from ground as capacitor C_N is charged up by a scaled copy of the positive-feedback current. The rise in V_n activates a discharging current at the membrane potential node that returns V_m to ground. The capacitor C_N is then slowly discharged by a passive leak current at the V_n node, which returns V_n linearly to ground. Meanwhile, the input current charges C_m back up to the threshold for firing, and the cycle of activity is periodically repeated. These waveforms were obtained with $V_{Na}^{th} = 2.50$ V, $V_{Na}^{max} = 1.20$ V, $V_R = 0.99$ V, and $V_{in} = 0.81$ V.

Figure 4—Input Output Characteristics of the Sodium-Potassium Neuron Circuit: Figure 4a shows that the firing frequency or spike rate of the neuron is linear with input current as long as the frequency of firing is not limited by the refractory period of the neuron. The data displayed for Figure 4a were taken with $V_{Na}^{th} = 2.50$ V, and $V_{Na}^{max} = 1.72$ V, for all curves.

Figure 4b shows the refractory period t_{ref} as a function of V_R, for a given input current I_{in}. In subthreshold, t_{ref} decreases exponentially with V_R. Data for Figure 4b were taken with V_{Na}^{th} = 2.50V, $V_{Na}^{max} = 1.72$, and $V_{in} = 1.15$.

Figure 5—The Sodium-Leak Neuron Circuit: The voltage, V_m, is the membrane potential, and the voltage V_h on capacitor C_H is the voltage that determines the state of refractoriness of the neuron. The bias voltages V_L, V_D and V_R set the threshold for firing, pulse width, and refractory period of the action potential, respectively. The input V_{in} is capacitively coupled to the circuit by capacitor C_C. An action potential is fired on every positive edge of a square-wave input, as long as the period of the input is greater than the neuron's refractory period.

Figure 6—Circuit Waveforms for the Sodium-Leak Neuron Circuit: In response to a positive edge of sufficient height at the input, the positive feedback in the circuit is activated, so the membrane potential, V_m, is driven from ground to V_{DD}. The capacitor C_H is then discharged from V_{DD} by a current source that is switched on when V_m reaches V_{DD}; V_h falls linearly toward ground. Eventually, V_h gets close enough to ground, that the inhibitory leak current at the membrane potential node exceeds the excitatory positive feedback current; the leak current, then, discharges V_m to ground. When V_m is at ground, the discharging current source at the V_h node is switched off and a charging current source is switched on. The charging current source starts charging C_H back up toward V_{DD}, so V_h rises linearly toward V_{DD}. After V_h has reached V_{DD}, the cycle of activity repeats again on the next positive edge in the input. These waveforms were obtained with $V_L = 1.516$, $V_D = 0.656$, $V_R = 4.40$, and V_{in} being a square-wave input of frequency 100 Hz and step height 2.630 V. Note that these waveforms are representative of a case where the period of the input is greater than the neuron's refractory period.

Figure 7—Threshold Voltage Characteristics for the Sodium-Leak Neuron Circuit: The threshold voltage, V_{TH}, is the height of the smallest positive step at the input that can cause an action potential. The threshold is linear with V_L for subthreshold values of V_L and deviates from linearity for above-threshold values of V_L. The data above were taken for $V_D = 0.502$ V, $V_R = 4.63$ V, with the input being a square wave of frequency 0.91 Hz.

Figure 8—Pulse Width Characteristics for the Sodium-Leak Neuron Circuit The pulse width, t_p, decays inversely with I_D, and thus exponentially with V_D for subthreshold values of V_D. The data above were taken for $V_L = 1.50$ V, $V_R = 4.63$ V, with the input being a square wave of frequency 0.91 Hz.

Figure 9—Refractory Period Characteristics for the Sodium-Leak Neuron Circuit Figure 9a shows the frequency halving behavior of the sodium-leak neuron circuit. As the period of the square wave input is less than the refractory period of the neuron, the circuit fires an action potential only on every other positive edge of the square-wave. The refractory period, t_R, is the inter-pulse interval at which frequency halving just begins to occur. Figure 9b shows that the refractory period, t_R, increases exponentially with V_R for subthreshold values of V_R. The data above were taken for $V_L = 1.50$V, with the input being a square wave of step height 2.57 V.

Figure 10—The Axon Delay Line The figure shows the input to an axon delay line and the outputs from the first five taps on the line. The delay line is built by having a chain of sodium-leak neurons coupled to one another via inverters . Each output is delayed from its predecessor by a pulse-width. The curves have been offset for clarity. The input p.p. value is 2.240 V and the pulse-widths are between 30 and 50 ms.

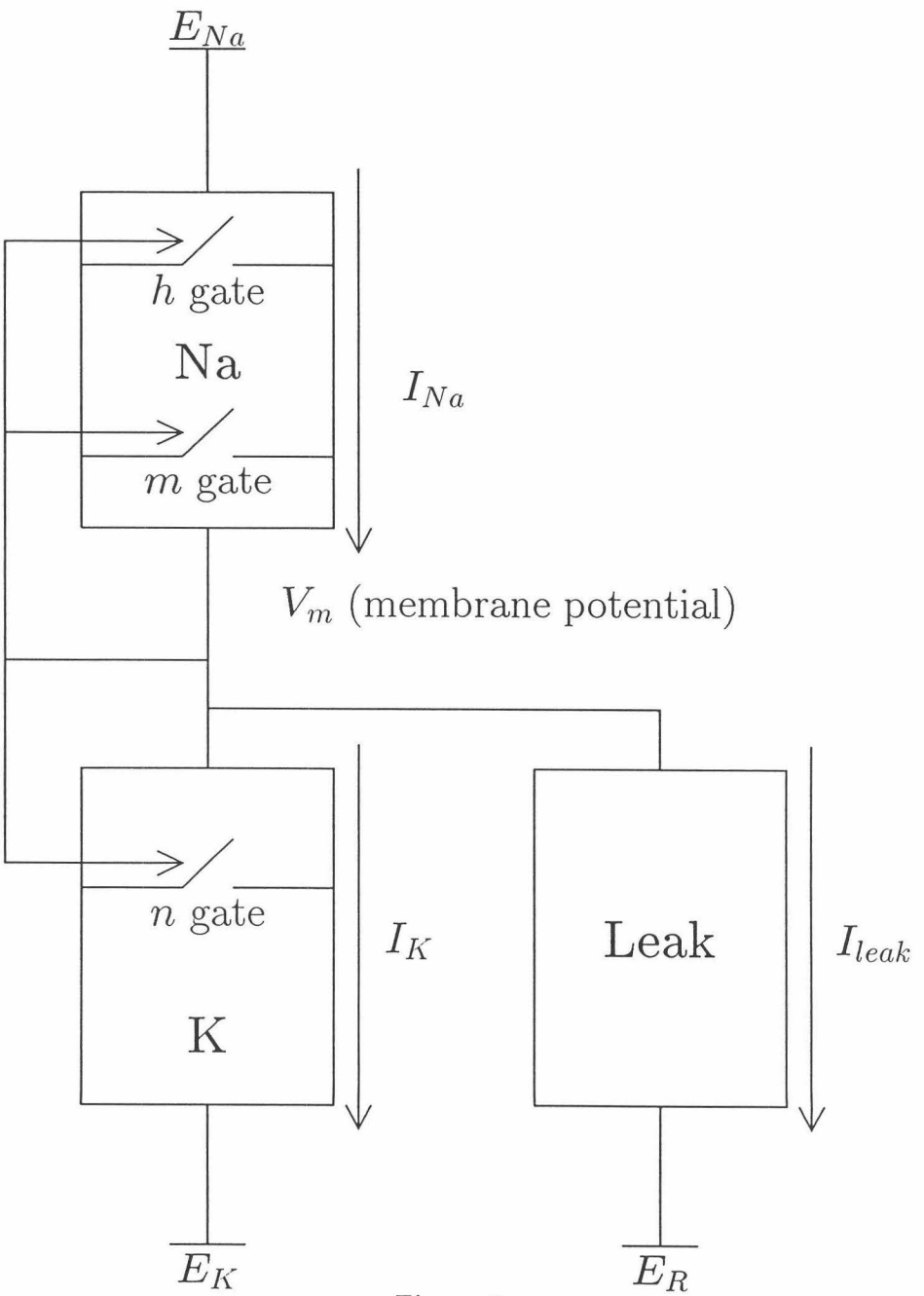
E_{Na}
h gate
Na
m gate
I_{Na}
V_m (membrane potential)
n gate
K
I_K
Leak
I_{leak}
E_K
E_R

Figure 1

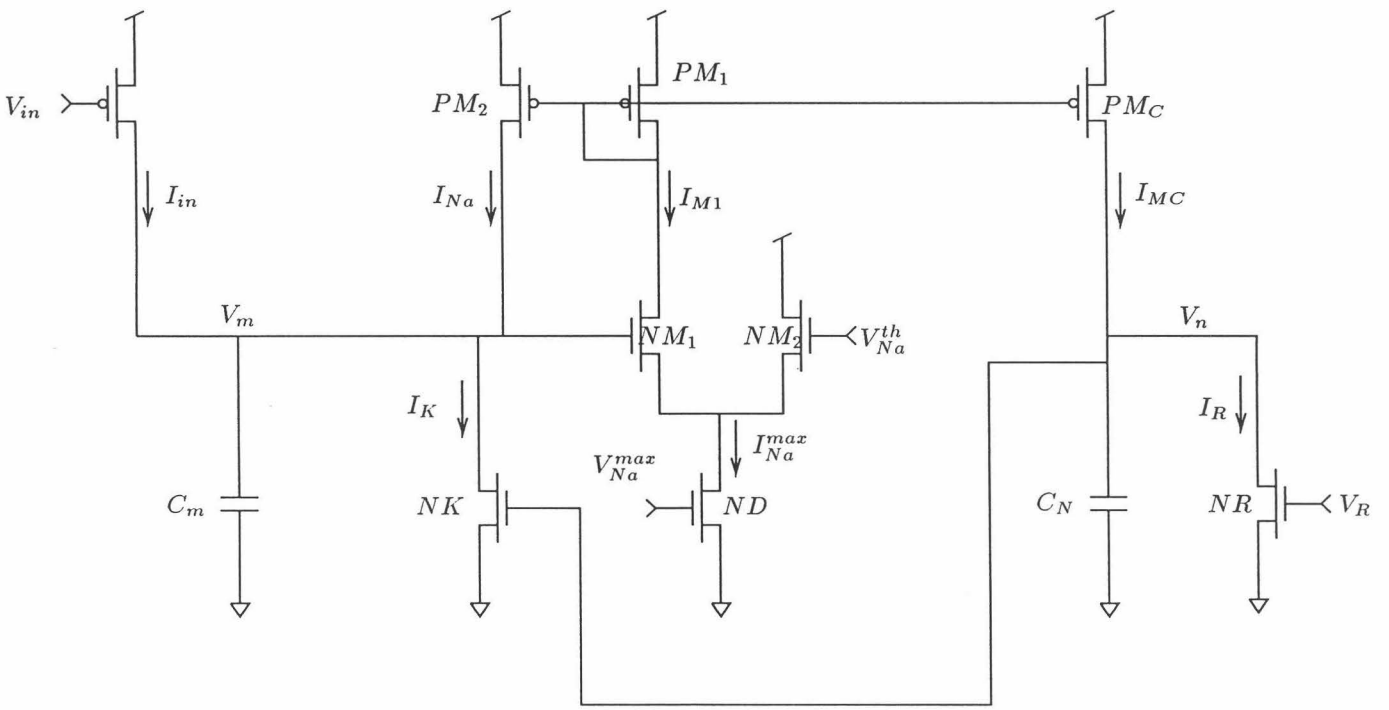
V_{in}
PM_2
PM_1
PM_C
I_{in}
I_{Na}
I_{M1}
I_{MC}
V_m
NM_1
NM_2
V_{Na}^{th}
V_n
I_K
I_{Na}^{max}
V_{Na}^{max}
I_R
C_m
NK
ND
C_N
NR
V_R

Figure 2

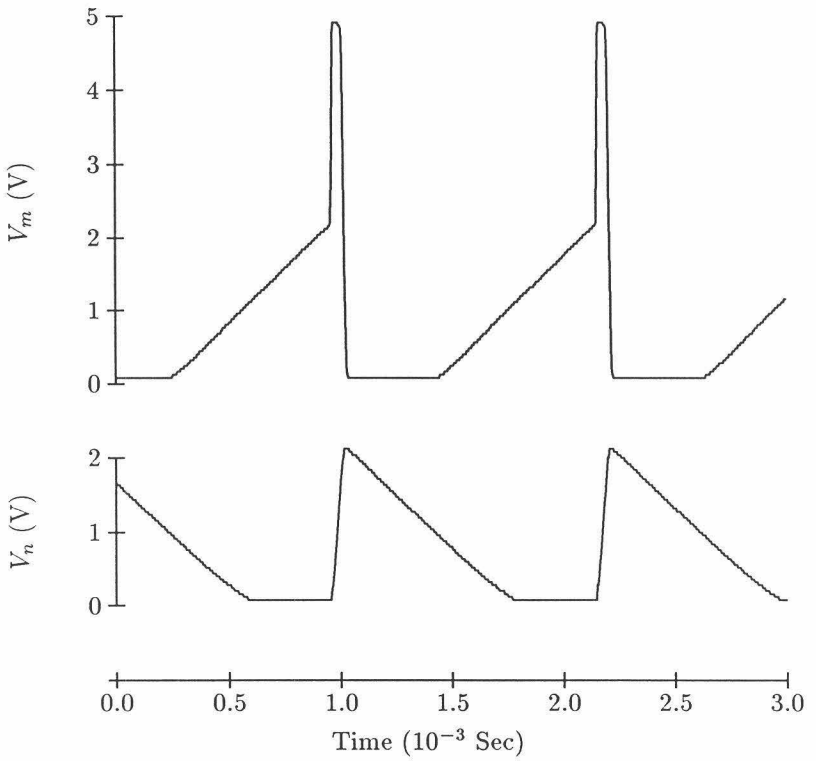

Figure 3

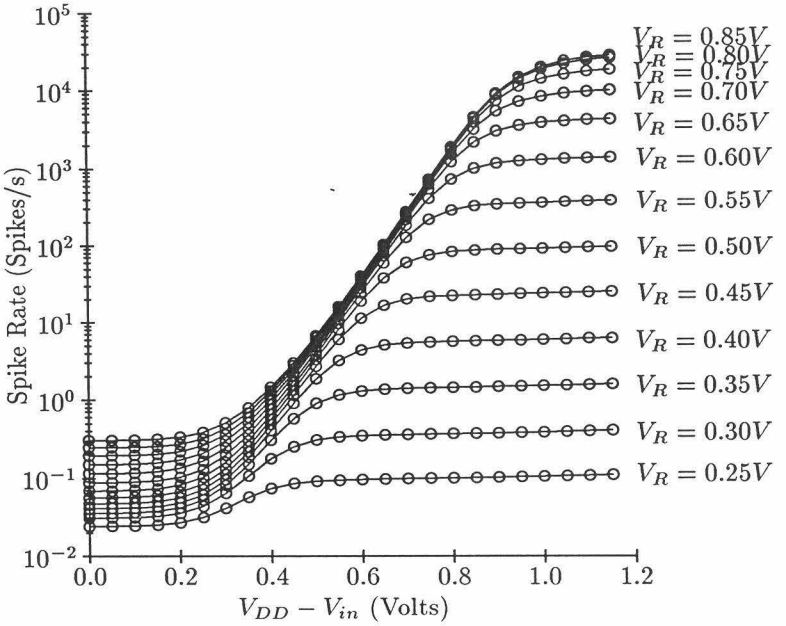

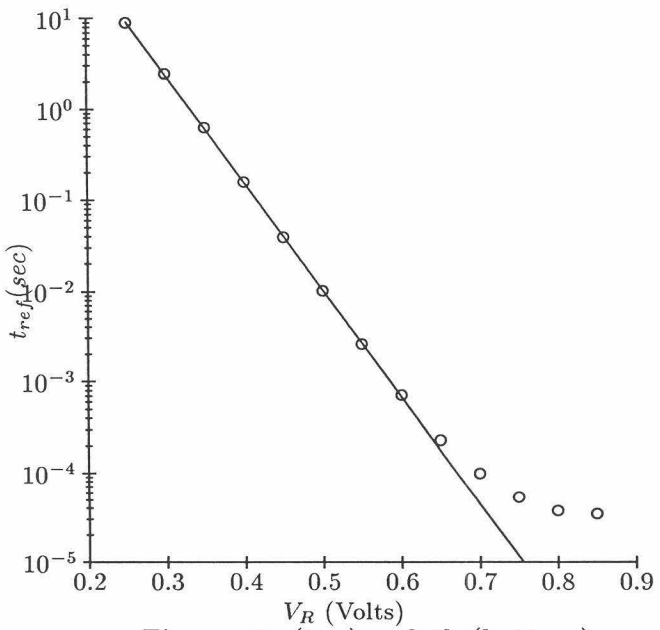

Figures 4a (top) and 4b (bottom)

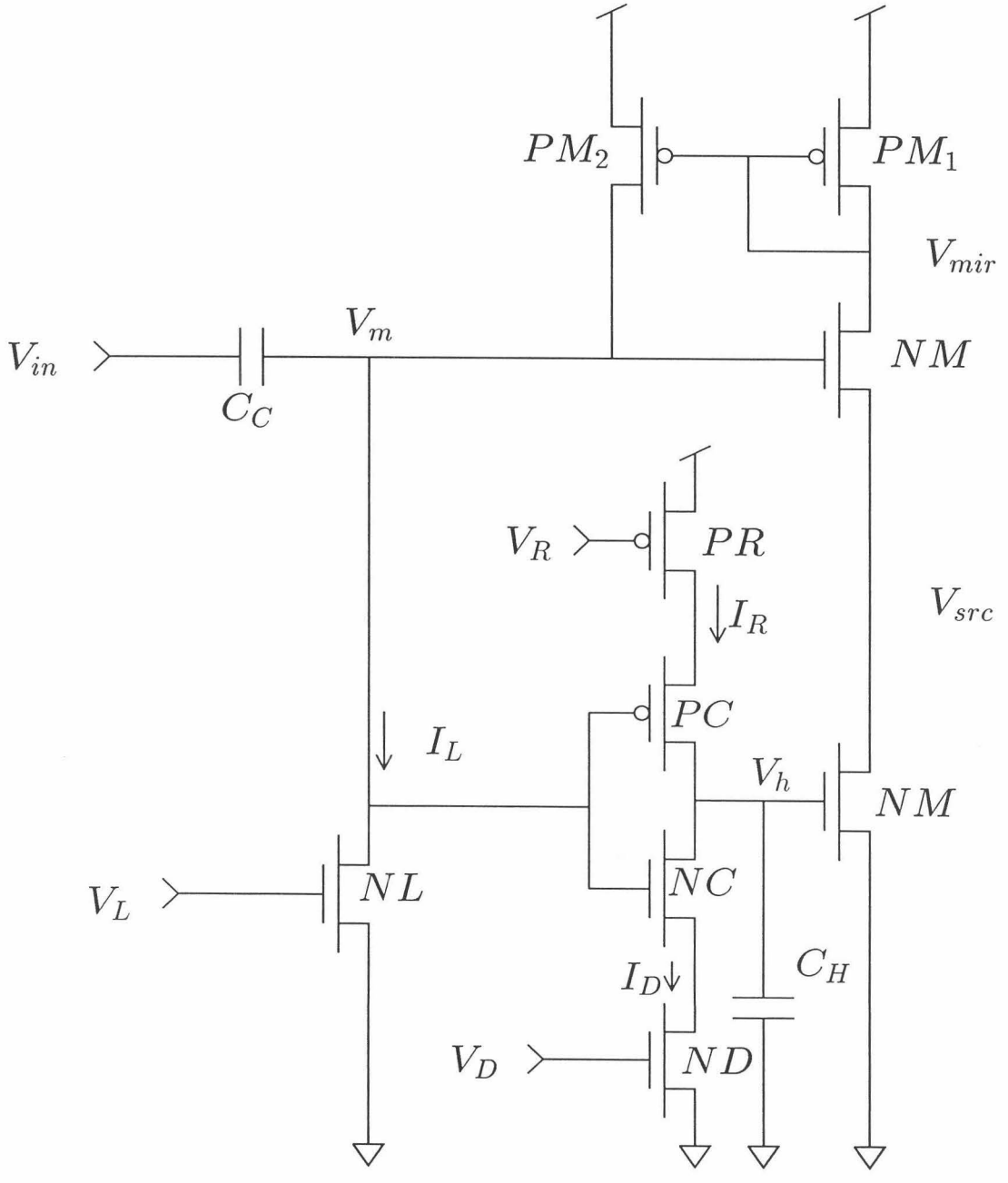
PM_2
PM_1
V_{mir}
V_{in}
V_m
C_C
NM
V_R
PR
I_R
V_{src}
PC
I_L
V_h
NM
V_L
NL
NC
I_D
C_H
V_D
ND

Figure 5

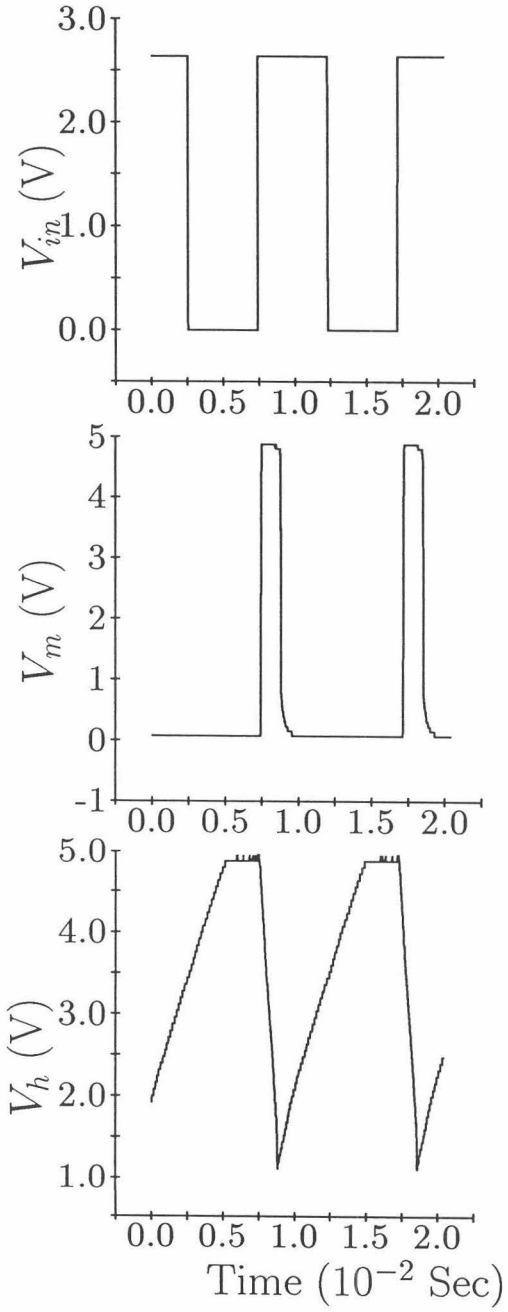
3.0
2.0
1.0
0.0
V_{in} (V)
0.0 0.5 1.0 1.5 2.0
5
4
3
2
1
0
-1
V_m (V)
0.0 0.5 1.0 1.5 2.0
5.0
4.0
3.0
2.0
1.0
V_h (V)
0.0 0.5 1.0 1.5 2.0
Time (10^{-2} Sec)

Figure 6

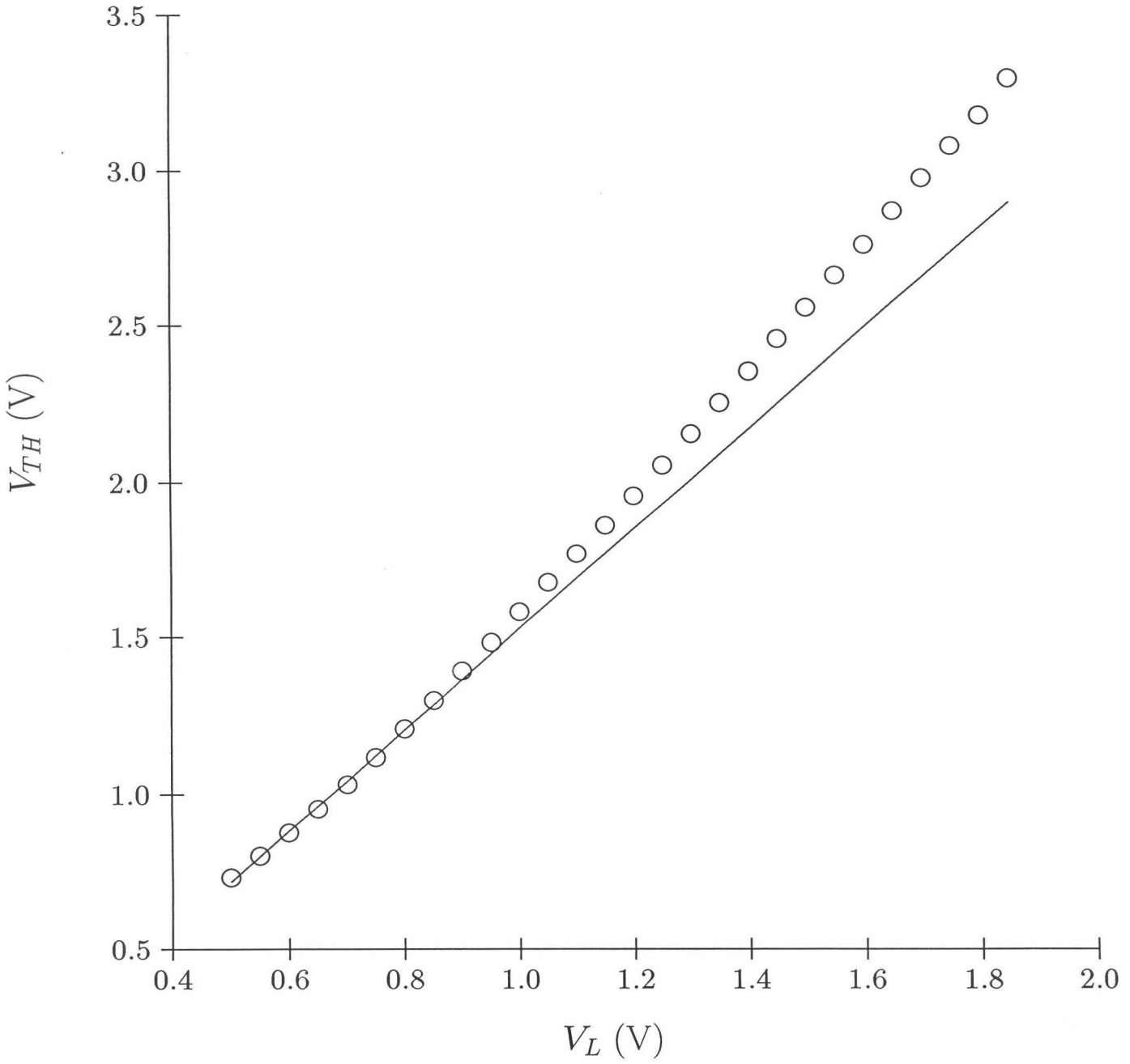

Figure 7

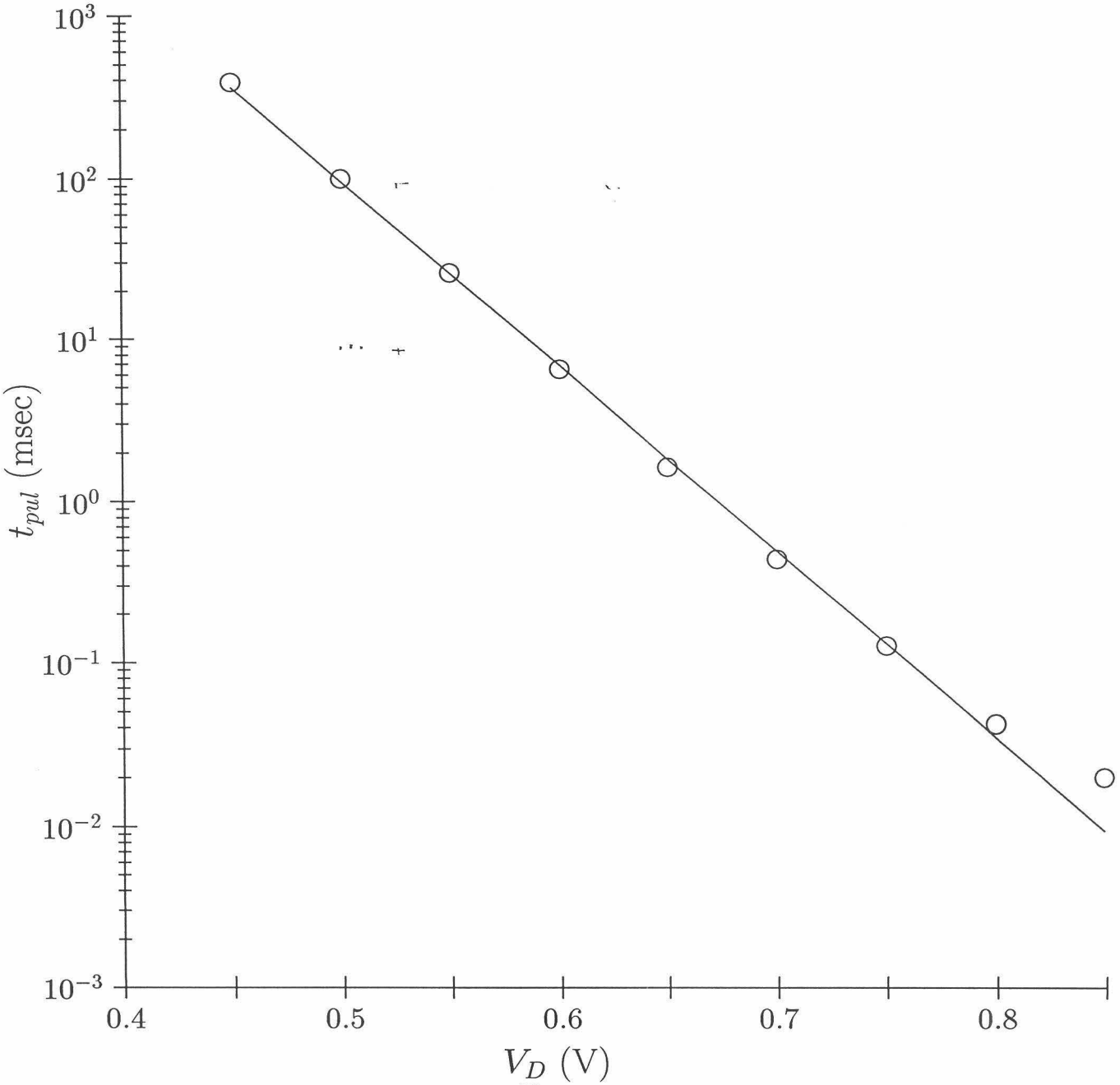

Figure 8

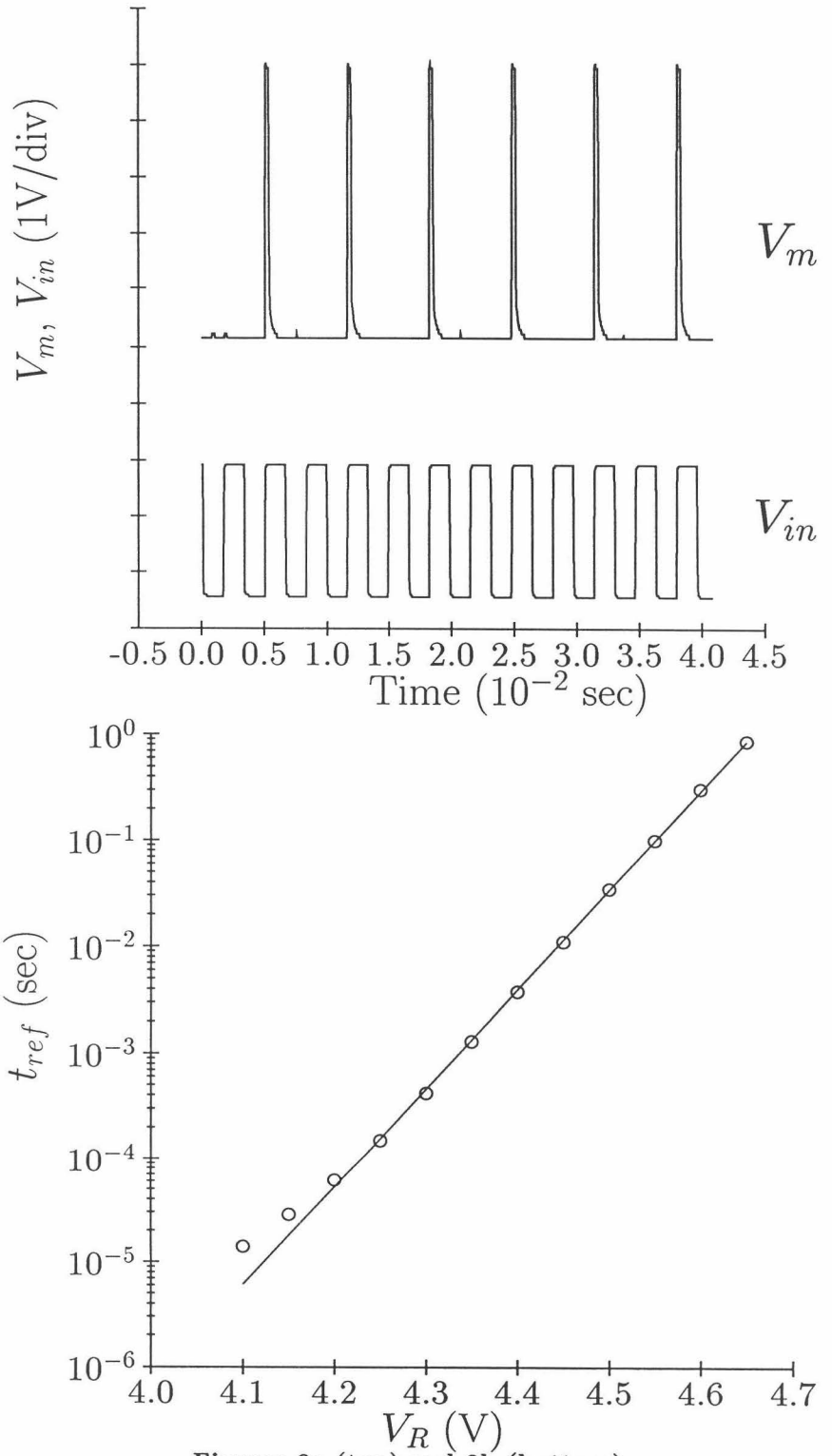

Figures 9a (top) and 9b (bottom)

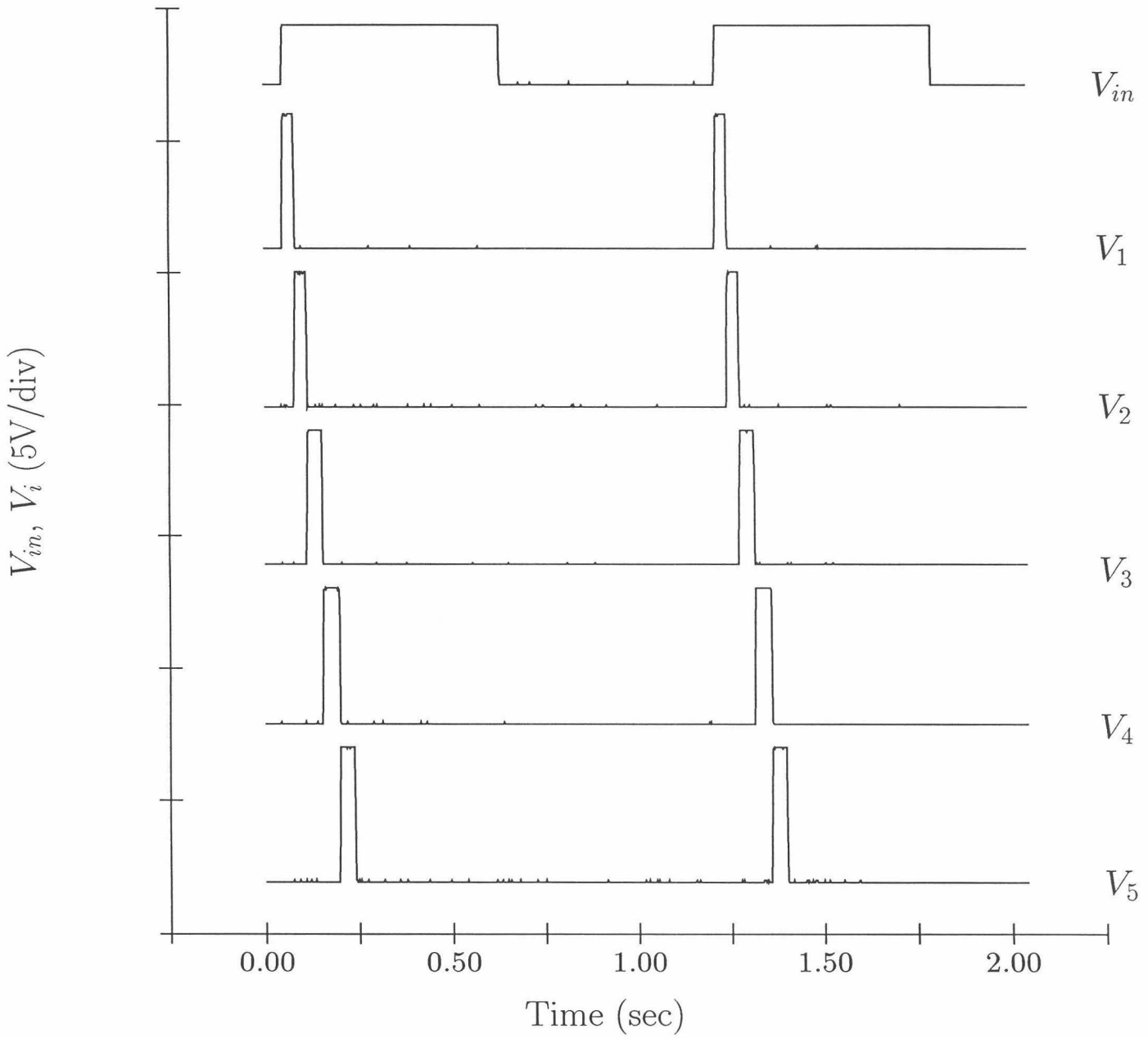

Figure 10